Eur Biophys J (2006) 35: 328–339
DOI 10.1007/s00249-005-0038-2

ARTICLE

Catherine Barentin · Yasuji Sawada · Jean-Paul Rieu

An iterative method to calculate forces exerted by single cells and multicellular assemblies from the detection of deformations of flexible substrates

Received: 21 July 2005 / Revised: 5 October 2005 / Accepted: 7 December 2005 / Published online: 11 January 2006

Abstract We present a new method for quantification of traction forces exerted by migrating single cells and multicellular assemblies from deformations of flexible substrate. It is based on an iterative biconjugate gradient inversion method. We show how the iteration and the solution are influenced by experimental parameters such as the noise on deformations σ_{XY}, and the mean depth of recorded deformations Z_M. In order to find the validity range of our computational method, we simulated two different patterns of force. The first artificial force pattern mimics the forces exerted by a migrating *Dictyostelium* slug at a spatial resolution of $\Delta = 20$ μm (Rieu et al. in Biophys J 89:3563–3576, 2005) and corresponds to a large and spread force field. The second simulated force pattern mimics forces exerted by a polarized fibroblast at discrete focal adhesion sites separated by $\Delta = 4$ μm. Our iterative method allows, without using explicit regularization, the detailed reconstruction of the two investigated patterns when noise is not too high ($\sigma_{XY}/u_{max} \leq 6\%$, where u_{max} is the maximal deformation), and when the plane of recorded deformations is close to the surface ($\Delta/Z_M \geq 4$). The method and the required range of parameters are particularly suitable to study forces over large fields such as those observed in multicellular assemblies.

Keywords *Dictyostelium* slugs · Elastic substrates · Traction forces · Regularization methods · Iterative methods

Electronic Supplementary Material Supplementary material is available for this article at http://dx.doi.org/10.1007/s00249-005-0038-2 and is accessible for authorized users.

C. Barentin · J.-P. Rieu (✉)
Laboratoire de Physique de la Matière Condensée et Nanostructures, Université Claude Bernard Lyon I & CNRS, 43 Boulevard du 11 Novembre, 69622 Villeurbanne Cedex, France
E-mail: rieu@lpmcn.univ-lyon1.fr

Y. Sawada
Tohoku Institute of Technology, 35-1 Yagiyama-Kasumi, Taihaku, 983 Sendai, Japan

Introduction

The ability of cells to apply forces to its surrounding is critical for migration, embryogenesis and metastasis (Galbraith et al. 2002). For animal cells, the actin-myosin cytoskeleton transmits forces to the substratum at adhesion sites (Balaban et al. 2001; Beningo et al. 2001; Tan et al. 2003; Uchida and Yumura 2004; Reinhart-King et al. 2005). By coordinating the magnitude of forces and the strength of adhesions in different regions, the cell is able to extend or migrate in a specific direction (Lauffenburger and Horwitz 1996). Cell–substrate adhesion complexes composed of integrins are linked to the cytoskeleton through a series of proteins. They can be detected as dark areas in interference reflection microscopy (Abercrombie and Dunn 1975), by electron microscopy or with fluorescence labeling of proteins (Balaban et al. 2001; Tan et al. 2003; Uchida and Yumura 2004; Reinhart-King et al. 2005). As fluorescence techniques became common biological laboratory practices, our understanding of chemical communications, and of cell–cell and cell–substrate adhesions considerably improved over the past two decades. In a biological tissue, cell motion is still poorly understood because it depends not only on the cell–cell and cell–substrate adhesions but also on the chemical and mechanical signals the cell receives from neighbors. Experiments following cell trajectories in confined two-dimensional (2D) cell aggregates (Rieu et al. 2000), in epithelial monolayers (Haga et al. 2005) or in *Dictyostelium* aggregates and slugs (Dormann et al. 1996; Rieu et al. 2004) provided insight into the kinematics of large-scale collective reorganization of cells. However, to understand the collective tissue-like movement exhibited by cellular aggregates, one must understand in conjunction with kinematics observations how forces are transmitted to the substrate (Dallon and Othmer 2004).

Although important advances have recently been made in the engineering of flexible substrate, direct measurement of the mechanical forces exerted by single

cells or colonies of cells is not yet a conventional technique. The flexible substrate methods fall into two classes: (1) methods recording the deformations of flat elastic substrata containing markers and requiring subsequent force calculations (Dembo and Wang 1999; Schwarz et al. 2002; Butler et al. 2002) and (2) direct detection of forces through independent microfabricated elastic pillars of several micrometer height (Tan et al. 2003; Petronis et al. 2003; du Roure et al. 2005; Mohrdieck et al. 2005). A review of pioneering or alternative methods can be found in (Schwarz et al. 2002; Beningo and Wang 2002). The obvious advantage of the second method is that no complex calculations are necessary to obtain forces as each pillar behaves as an elastic spring: deflection is proportional to force. However, the method is technologically rather challenging. First, in order to fabricate the substrates, it is necessary to have access to photolithography facilities. Pillars are made by replica-molding in PDMS and the Young's modulus is adjusted by pillar geometry. Second, cells may spread down the height of the pillars, and, therefore, their deflection does not quantitatively reflect the applied traction force.

Due to these technological complications, the first method remains widely used. The observation of the substrate deformations is generally accomplished by tracking fluorescent beads embedded inside polyacrylamide substrates (Dembo and Wang 1999). Alternatively, the deformation of micropatterned PDMS substrates with a topographic modulation of 0.3 μm depth can be recorded by phase contrast microscopy (Balaban et al. 2001). The Young's modulus E of the elastic substrates is usually adjusted in the range 0.2–30 kPa in case of polyacrylamide substrate by changing the proportion of acrylamide and *bis*-monomers (Pelham and Wang 1997). Because the marker displacements near the substrate surface are much smaller than the film thickness, they can be evaluated under the assumption that the thick film behaves like an elastic halfspace, whose elastic Green functions are known (Landau and Lifshitz 1986). However, complex calculations are necessary to invert the system of coupled integral equations given by linear elasticity theory that relate the substrate deformations to the forces (Dembo and Wang 1999). It is well known that this inverse problem is ill-posed due to experimental noise on deformations and that regularization of the solution in general cannot be neglected under usual level of noise (Schwarz et al. 2002). This means that non-regularized solutions are expected to be really sensitive to small changes in the deformation data (Press et al. 1992, chap.18.0).

In case of flexible substrate experiments, regularization generally consists of adding a side constraint to the minimization of the usual χ^2-estimates that eliminates erratic solutions. In particular, Dembo and Wang use a side constraint to penalize large gradients of the force field. They also make an assumption that force is zero outside the cell boundary visualized by phase contrast microscopy (Dembo and Wang 1999). Details of the calculations can be found in a complicated mathematical paper (Dembo et al. 1996). This approach was simplified in the restricted case of isolated point sources of forces (Balaban et al. 2001; Schwarz et al. 2002). Computing the force field is sometimes so difficult that some authors used the raw displacements themselves with a simple calibration as a qualitative map of the local traction forces (Uchida et al. 2003). There is, therefore, a need for simplified methods even for single cells. Unconstrained methods are required if the precise localization of forces is difficult to assess because stress bearing elements may not be seen in a particular microscope configuration (e.g., rapid formation of thin filipodia in single cells, collapsed sheath area in *Dictyostelium* slugs, Rieu et al. 2004, 2005). A method that is able to calculate forces over large fields (i.e., to invert large matrix) is also necessary in case of multicellular assemblies like epithelium monolayers (du Roure et al. 2005).

We recently applied the flat polyacrylamide substrate method to the measurement of the forces exerted by migrating *Dictyostelium* slugs (Rieu et al. 2004, 2005). We first measured the displacement fields of the fluorescent beads embedded in the polyacrylamide gel induced by the migration of the slugs. Taking into account the advantage that slugs often have a linear trajectory, we averaged data in the moving slug frame in order to reduce noise and we calculated the forces using an iterative biconjugate gradient inversion method.

In the present work, we address the details of our computational method. We show the way in which the iteration and the solution are chosen and how experimental parameters such as the noise on deformations or the mean depth of recorded deformations affect the solutions. We simulated two different force patterns in order to determine the validity range of our computational method. The first artificial force pattern mimics the forces exerted by a migrating *Dictyostelium* slug (Rieu et al. 2004) and corresponds to a large and spread force field. Typically, the width of a slug is 150 μm, the length is 700 μm and the forces are calculated with a spatial resolution of about 20 μm. The second simulated force pattern mimics forces exerted by a polarized fibroblast at discrete focal adhesion (FA) sites separated by 4 μm. This pattern corresponds to sharp and discrete forces and allows us to study the applicability of our method to measure forces exerted by single cells.

Methods

The deformation field $u(r)$ inside a semi-infinite elastic medium caused by a distribution of forces $F(r')$ on the surface is described by a Fredholm integral equation of the first kind:

$$u_i(r) = \int dr'\, G_{ij}(r - r')\, F_j(r'). \quad (1)$$

Note that deformations are measured at positions $r=(x, y, Z_M)$ where Z_M is the mean bead depth from the surface, while forces are calculated on the surface at $r'=(x', y', 0)$. dr' is, therefore, a 2D integral. In Eq. 1, i and j refer to the components x,y,z of the vectors and G_{ij} are Green functions scaling as $(r-r')^{-1}$ (Dembo and Wang 1999; Landau and Lifshitz 1986). Point forces are calculated at the same (x, y) coordinates than measured deformations but on the surface ($z=0$). Here, we simulate force patterns without vertical forces ($F_z=0$). As a result, the in-plane displacements (u_x, u_y) become functions of (F_x, F_y) only. In experiments, the mean depth of recorded deformations Z_M is usually on the surface plane (i.e., $Z_M=0$; Schwarz et al. 2002; Butler et al. 2002), or close to the surface (i.e., $Z_M << |r-r'|$; Dembo and Wang 1999). As a result, the Green functions G_{xz}, G_{yz} can be neglected, and again only the in-plane displacements and forces need to be considered for a Poisson ratio $v=0.5$ (Dembo and Wang 1999). Our method is an unconstrained one (Butler et al. 2002): we do not impose the forces to be zero outside the slug area.

The integral equation from Eq. 1 becomes a set of linear equations, $u=GF$, in which $u=(u_x(r_1), u_y(r_1), u_x(r_2), u_y(r_2), ...)$, and $F=(F_x(r_1), F_y(r_1), F_x(r_2), F_y(r_2), ...)$ are $2N$-vectors and G is a $4N^2$-matrix (typically $N\sim 2\times 10^3$ and the matrix has more than 10^7 terms). To solve these equations, we run a numerical program based on iterative biconjugate gradient method generally used to invert large sparse matrix (Press et al. 1992) (chapter 2, p. 71–89, program "*linbcg*" and related subroutines). Of course, here the matrix is dense but this method is known to give good results especially for 2D problems. Direct solution of Eq. 1 in this case is hopeless since the matrix G is too large (Press et al. 1992) (chap 18.5, p 803–804). It takes typically 5 min to invert a 10^7 terms matrix using a personal computer with a 1.6 GHz microprocessor.

The main difficulty in the inversion of type-1 Fredholm integral equation lies in the computational technique to eliminate the non-physical or erratic solutions (here forces) of the system. These non-physical solutions of high frequency and possible high amplitude produce a displacement field not distinguishable from the initial displacements. Here, we do not use explicit side constraints to regularize the solutions. We record every iteration of the force field from an initial input of null force. As the iterative inversion method gives only an approach to the solution of the inverted matrix, the force field progressively builds up itself iteration after iteration. For every iteration (#), we calculate several parameters used to eliminate non-physical or erratic solutions using criteria described below. These parameters include:

- The mean relative error on the calculated displacements $E_r=\langle((u_x-c_x)^2+(u_y-c_y)^2)^{1/2}\rangle$ (in μm, where $\langle\ \rangle$ is a mean over all sites) which characterizes the difference between the measured displacements u and the calculated displacements $c=GF$.
- The mean force $\langle F_{in}\rangle$ or mean stress $\langle P_{in}\rangle$ inside the slug area which are often used in regularization methods to eliminate erratic solutions of high amplitude (Schwarz et al. 2002) and the mean force or stress outside $\langle F_{out}\rangle$ or $\langle P_{out}\rangle$. These parameters provide supplementary control for the level of force error in the experiments.
- The ratio between forces outside and inside: $\phi_{ext}=\langle F_{out}\rangle/\langle F_{in}\rangle$.

In the case of simulations, we know the original force pattern and, therefore, the error on the calculated forces. We define the force deviation ΔF in the slug area as:

$$\Delta F=\frac{\langle((F_x(\#)-F_{0x})^2+(F_y(\#)-F_{0y})^2)^{1/2}\rangle}{\langle|F_0|\rangle},$$

where F_0 is the original force. The absolute optimal # and solution are then obtained at the minimum of ΔF. The comparison between the parameters shows that in case of extended force fields (here slug patterns), the minima of ΔF and ϕ_{ext} coincide so that ϕ_{ext} is a good criterion to choose the optimal # and evaluate the force error (see Results). This study also shows that a more general criterion is given by the displacement error E_r: the optimal # is chosen when E_r reaches the experimental error for large Δ/Z_M (typically ≥4), or when E_r is minimal within the range 1–10# for low Δ/Z_M.

The experimental noise on displacement (simply referred to as "noise") is comprised of an in-plane component σ_{XY} due to lateral resolution and a vertical component σ_Z due to the finite depth of field of the objective. We simulate in-plane noise only as both types of noise have roughly the same effects provided that they are both Gaussian. We operate, therefore, in our simulations as follows: starting from the original force pattern, we use Eq. 1 to calculate the displacement field at different depths Z_M. We add Gaussian noise having a standard deviation σ_{XY} to the displacement field and then we run our numerical program to reconstruct forces.

Results

Simulated *Dictyostelium* slug force pattern

Figure 1a shows an artificial stress pattern (force per unit area) that mimics the force exerted by a migrating *Dictyostelium* slug (Rieu et al. 2004). The slug width is 140 μm and the slug length is 640 μm. This type of slug generally moves forward in a straight direction (i.e., here, from left to right) with a fairly constant velocity and shape. The stress pattern has the following typically characteristic properties: large perpendicular stress directed outward on the peripheral sides, friction in the tip and in the tail (directed forward) and traction (directed backward) in the central prespore area (Rieu et al. 2004). Stress also exists in the trail of the slug as

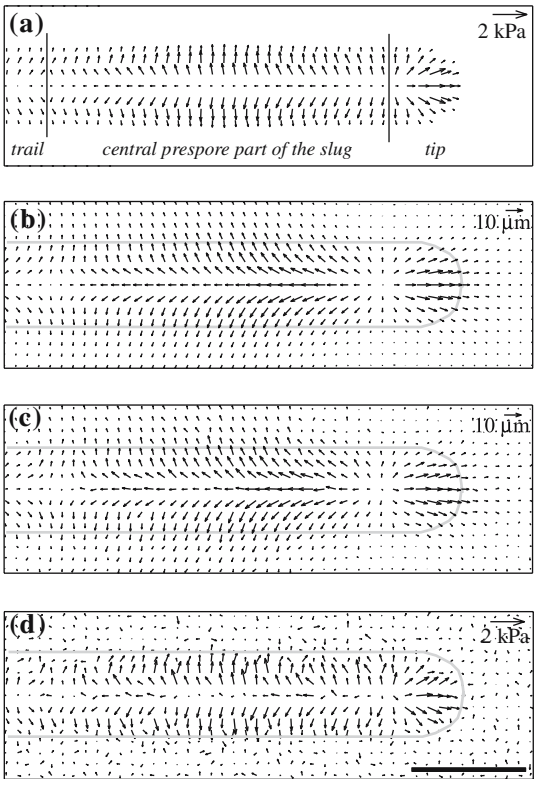

Fig. 1 **a** Artificial stress pattern mimicking the force exerted by a migrating *Dictyostelium* slug of 670 µm length with large perpendicular stress directed outward toward the peripheral sides of the slug, parallel friction (oriented *forward*) in the tip and in the trail of the slug and parallel traction (oriented *backward*) with an oscillatory component in the central prespore part of the slug. **b** Resulting displacement field calculated at $Z_M = 5$ µm below the surface. **c** The same displacement field as (**b**) but with a Gaussian noise of standard deviation $\sigma_{XY} = 0.45$ µm added. Slug external boundary is represented by the *thick gray line*. **d** Reconstructed stress field after iteration 4 calculated from the previous displacement field (**c**). *Bar* 200 µm

found experimentally (Rieu et al. 2005). Typical stress is 500–1,000 Pa for the friction and perpendicular forces, 200 Pa in the traction area. In this traction area, we introduce a parallel stress modulation $f = f_{dc} + f_{ac} \times -\cos(2\pi x/\lambda + \phi)$, keeping the total traction stress constant and balanced by friction stress. We used here a ratio $p = f_{ac}/f_{dc} = 0.5$. This modulation simulates the possible existence of waves of forces associated with the waves of cell velocity that have been found in strains of *Dictyostelium* (Dormann and Weijer 2001) and in 2D slugs (Rieu et al. 2004). One test of our force reconstruction will be to see whether these waves can be retrieved when noise increases.

Stresses are measured at a 20 µm interval on a grid and deformations are computed at the same sites. This pattern is typically obtained experimentally when recording the deformation induced by migrating slugs of 400–1,000 µm length with a 20× objective and averaging data over time in the moving slug frame (Rieu et al. 2004). It may also correspond to experiments where deformation data is collected using micropatterned surfaces (Balaban et al. 2001; Schwarz et al. 2002) or image correlation methods (Butler et al. 2002; Marganski et al. 2003).

Figure 1b shows the displacement resulting from this force pattern at $Z_M = 5$ µm below the surface, using a Poisson modulus of 0.5 and a Young modulus E of 5 kPa. Note that the deformations depend only on the ratio of the force over E, so that E can be adjusted in order to obtain large deformations still smaller than the grid spacing. Note also that the displacements decrease with Z_M. The largest vector displacement is for instance $u_{max} = 12.5$ µm at $Z_M = 2.5$ µm, and $u_{max} = 6.7$ µm at $Z_M = 10$ µm. In order to simulate the experimental noise inherent to data collection, the displacement field of Fig. 1b is subject to in-plane Gaussian noise with a standard deviation σ_{XY}. Experimentally, we measured typically $\sigma_{XY} \sim 0.15$ µm when averaging displacements over time and $\sigma_{XY} \sim 0.3$–0.5 µm for raw data at given times (Rieu et al. 2005). We then investigate the effect on reconstructed stress fields of noise levels between 0.01 and 0.6 µm at various depths Z_M. Figure 1c shows the displacement field of Fig. 1b plus a Gaussian noise with a standard deviation of 0.45 µm, and Fig. 1d displays the reconstructed stress field for such high level of noise. We will examine in detail the features of the reconstructed stress fields as a function of Z_M and σ_{XY}, but note that the pattern of Fig. 1d is very similar to the original one (Fig. 1a) except for the noise inside and outside the area occupied by the slug.

In Fig. 2, we present the reconstructed stress fields obtained with our iterative matrix inversion code at various iterations steps (#). The different parameters that allow the choice of the optimal solution, as a function of the # are plotted in Fig. 3. For $Z_M = 5$ µm and a noise level of $\sigma_{XY} = 0.15$ µm the optimal solution is obtained after six iterations as given by the minimum of the force deviation ΔF at 15% (Fig. 3a). The optimal reconstructed stress pattern at #6 (Fig. 2b) is, of course, much more similar to the original one (Fig. 1a) than with the same Z_M but $\sigma_{XY} = 0.45$ µm (Fig. 1d). The stress noise outside the slug area is low and the slug boundary is sharp. At lower iteration number (i.e., #1–3), the stress pattern is still not fully reconstructed and resembles the deformation pattern in the sense that there the stress vectors do not vanish sharply after the slug boundary (Fig. 2a). The mean stress $\langle P_{in} \rangle$ inside the slug area increases until 6–7 iterations and then remains constant, whereas the remaining stress outside the slug area $\langle P_{out} \rangle$ continues to increase until 13–14 iterations (Fig. 3c). As a consequence, ΔF also increases until 13–14 iterations (Fig. 3a) and the proportion of external stress ϕ_{ext} shows a minimum at five iterations (Fig. 3a). Although ϕ_{ext} and ΔF do not reach the minima at exactly the same iteration, the similarity between the two curves is striking. This indicates that at least for such stress pattern (smooth central stress area and sharp interface), the minimal ϕ_{ext} provides a good criterion for the optimal solution. A more general criterion without

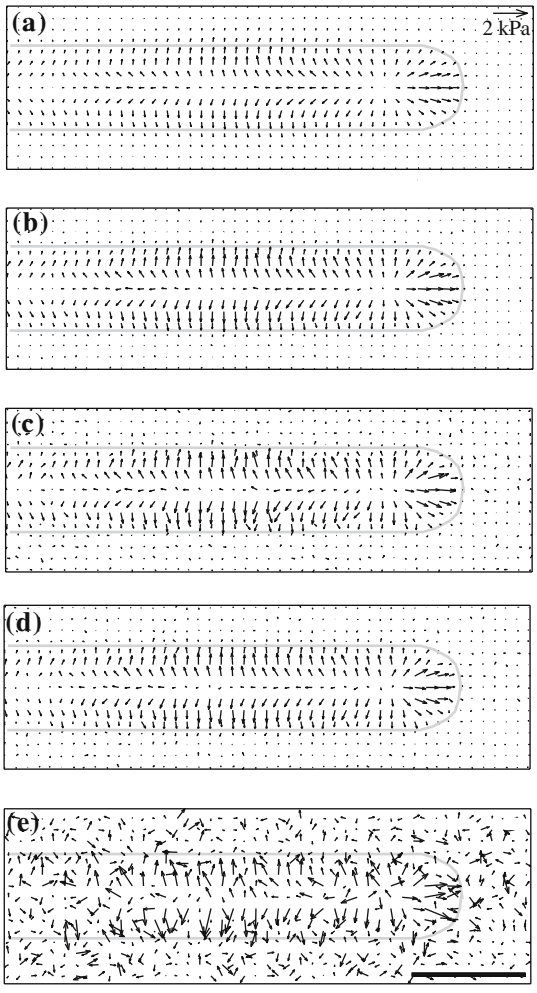

Fig. 2 Stress fields calculated for various deformations sets and at different iteration numbers (#) are presented: **a** $Z_M = 5$ μm, $\sigma_{XY} = 0.15$ μm, #3; **b** $Z_M = 5$ μm, $\sigma_{XY} = 0.15$ μm, #6; **c** $Z_M = 5$ μm, $\sigma_{XY} = 0.15$ μm, #20; **d** $Z_M = 10$ μm, $\sigma_{XY} = 0.075$ μm, #7; **e** $Z_M = 10$ μm, $\sigma_{XY} = 0.075$ μm, #25. Slug external boundary is represented by the *thick gray line*. Stress scale is the same for all patterns. *Bar* 200 μm.

any prior knowledge of the solution is given by the mean error E_r. For low Z_M, we find that E_r almost continuously decreases toward zero after iterations. This means that the code is able to find a solution that accommodates any added noise of standard deviation σ_{XY}. Of course, this is not physically amenable. Hence, we stop the iteration process at $E_r = \sigma_{XY}$. This criterion gives the iteration range 6–8, which is similar to the previous estimate (#5 for the minimum of ϕ_{ext}, #6 for the minimum of ΔF). Solutions at iterations 5–8 are quite difficult to distinguish from each other (data not shown).

The error landscape is very different for larger Z_M (i.e., $Z_M = 10$ μm, Fig. 3b), the error E_r is a non-monotonic function of # and presents a series of minima separated by large peaks (note the log scale in Fig. 3b). The first main minimum of E_r at #8 is close to the minima of ϕ_{ext} at #7 and ΔF. At this optimal iteration, the reconstructed stress pattern is reasonably close to the original one (Fig. 2d), but the force deviation ΔF = 23% is larger than the one found for $Z_M = 5$ μm although the added noise is here smaller ($\sigma_{XY} = 0.075$ μm). E_r does not reach this level of added noise. The absolute minimum of E_r within the range of 1–30 iterations is in fact reached at #25. However, at this iteration, the values of ΔF, ϕ_{ext} and $\langle P_{in} \rangle$ are much larger than those at #7, and the solution is completely erratic (Fig. 2e). We never found optimal solutions at higher iterations for a level of noise consistent with experiments. The criterion using E_r to find the optimal iteration is, therefore, to take the first main minimum of E_r within the range of 1–10 iterations. Again, the minimum of ϕ_{ext} provides a very good criterion for selecting a solution (neither too smooth nor erratic) and to evaluate the force deviation in the experiments.

After choosing the solution, we now examine quantitatively the effect of Z_M and σ_{XY} on the reconstructed solution of the simulated slug shown in Fig. 1. For more clarity, we will present only the 1D parallel and perpendicular stress profiles rather than the stress pattern. Note that the perpendicular profile is less noisy because it is calculated by averaging over half of the slug length, while the parallel profile which corresponds to the central line profile was not averaged. Figure 3c–d shows such profiles for different depths Z_M and for a similar Gaussian noise of standard deviation $\sigma_{XY} = 0.15$ μm. The agreement with the original stress patterns is better for lower Z_M (i.e., $Z_M = 2.5$ and 5 μm). For larger Z_M (i.e., $Z_M = 10$ and 20 μm), the parallel stress component is still reasonable although more sensitive to the noise. The oscillations in the central traction area is always retrieved (Fig. 3c). However, the perpendicular stress profile is considerably spread at large Z_M, the maximum of perpendicular stress is lower and stress exists outside the slug area (Fig. 3d). To a lesser extent, this loss of sharpness exists also in the tip friction peak of the parallel component (Fig. 3c).

In Fig. 3e, f, we study the effect of the noise σ_{XY} at a constant $Z_M = 5$ μm. As expected, increasing the noise on the displacement field increases the noise on the stress profiles. However, even for the larger value $\sigma_{XY} = 0.6$ μm, the oscillations in the central traction area are clearly visible and the perpendicular stress profile did not lose its sharpness. For larger Z_M, increasing σ_{XY} tends to worsen the effect of spreading the perpendicular component.

Changing all the distances in the Green function by the same factor (i.e., rescaling Z_M and Δ) only changes the amplitude of the force or stress, not the qualitative pattern. The results of the simulations and in particular the relative force deviation ΔF may be transposed at any scale and depends only on the dimensionless parameter Δ/Z_M. In the same way, changing the noise σ_{XY} and the amplitude of the deformations in the same proportion do not change ΔF. Therefore, we present in Fig. 6 the force deviation ΔF as a function of the noise to signal ratio σ_{XY}/u_{max} for different values of Δ/Z_M, in order to compare the results of the simulated slug force pattern with other patterns (bullets correspond to the FA sim-

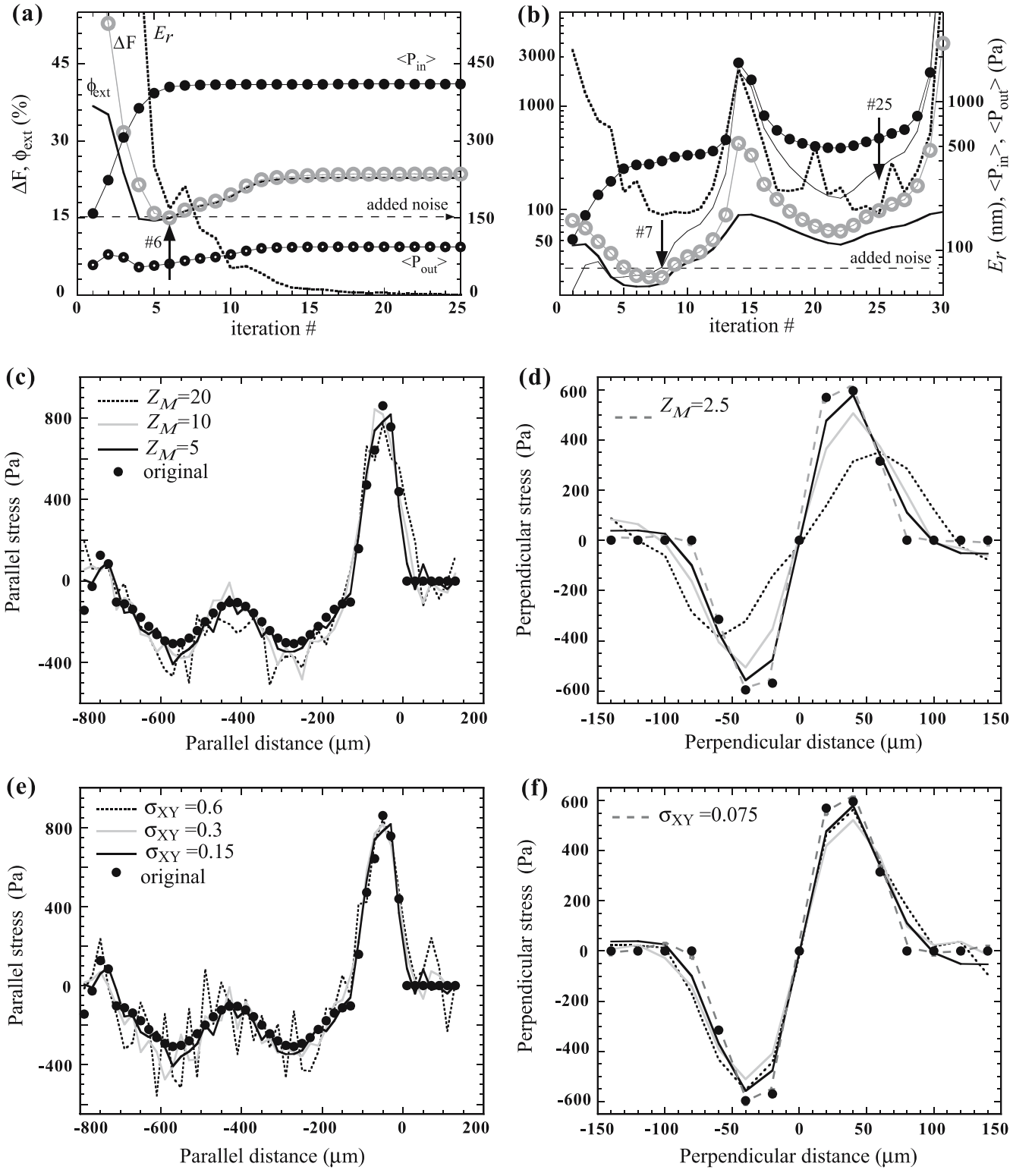

Fig. 3 **a** Error landscape as a function of the iteration number # at $Z_M = 5$ μm and $\sigma_{XY} = 0.15$ μm. **b** Error landscape (in log scale) at $Z_M = 10$ μm and $\sigma_{XY} = 0.075$ μm (here, $\langle P_{out} \rangle$ is not displayed for more clarity). Legend is displayed above (**a**). *Arrows* indicate optimal # or minima in the error landscape discussed in the text. *Dotted line* is the level of Gaussian noise (in nm) added to deformation field. **c**, **d** Effect of a Gaussian noise of standard deviation $\sigma_{XY} = 0.15$ μm on the recalculated **c** parallel stress profile and **d** perpendicular stress profile as a function of parallel and perpendicular directions respectively for different values of Z_M (in μm). In **c** $Z_M = 2.5$ μm is not displayed for more clarity but is almost similar to the original data. **e** Parallel stress profiles and **f** perpendicular stress profiles as a function of parallel and perpendicular directions respectively for different values of the Gaussian noise on displacements σ_{XY} (in μm). $Z_M = 5$ μm for all curves of (**e**, **f**). In **e** $\sigma_{XY} = 0.075$ μm is not displayed for more clarity but is almost similar to the original data

ulation discussed below). We also indicate the optimal #. The noise was normalized by the maximal deformation $u_{max} = 8.6$ μm at $Z_M = 5$ μm. Curves are stopped when the noise level makes the force reconstruction hardly distinguishable from noise level or when the optimal iteration is at the limit #3∼4. Of course, the higher the optimal iteration is, the smaller the ΔF. As previously noted, the mean force deviation increases considerably with Z_M even for lower noise. For $\Delta/Z_M = 4$ ($Z_M = 5$ μm), which is a reasonably accessible value experimentally, the force deviation is always smaller than 30% and the forces are only spread a little for a loud noise level (Figs. 1d, 3e, f). We can conclude from this first simulated force pattern that at a lateral resolution $\Delta = 20$ μm, explicit regularization is clearly not needed to find the details of the pattern if the noise to signal ratio is smaller than 7% and Z_M is sufficiently low ($Z_M \leq 5$ μm). To find the overall pattern and mean values (mean friction, mean traction values, Rieu et al. 2005), $Z_M = 10$ μm is, however, sufficient.

Dictyostelium slug experimental force field

In order to demonstrate the efficiency of our iterative method at a multicellular scale when displacement data is properly collected, we present the experimental force field of a 590-μm long migrating *Dictyostelium* slug. We previously calculated forces for data averaged in the moving slug frame in order to reduce the experimental noise on deformations (Rieu et al. 2004) or in order to study very long slugs larger than the field of view (Rieu et al. 2005). Here, we show that our method works also for non-averaged data.

Wild-type *Dictyostelium* slugs were developed at 21°C on flexible polyacrylamide gel substrates (10% acrylamide, 0.03% bis, Bio-Rad) coated with type I collagen and that contains 4-μm fluorescent beads (Molecular Probes) as previously described (Rieu et al. 2004). The Young's modulus of the elastomer was measured at 8.5 kPa and the Poisson ratio v was taken as 0.5 (Dembo and Wang 1999). We visualized simultaneously with a confocal microscope (Olympus IX70-KrAr-SPI, Japan) the ventral portion of the slug and the beads (see Movie 1, which can be published as an Electronic Supplemental Material, contact the editor). We selected a field of view with the slug approaching on the side and we took the initial image as the undisturbed position to calculate the displacement vector of each bead using our own codes (Rieu et al. 2005). The experimental displacement field at $Z_M = 5$ μm (Fig. 5a) is qualitatively similar to the simulated field of Fig. 1. An enlarged part of the field is displayed in Fig. 5b superimposed with the fluorescence image showing beads (after thresholding). Most of the beads are well separated with a mean distance of 21.7 μm between them that is closed in the bead spacing used in the previous slug simulation ($\Delta = 20$ μm).

Deformations are measured at (x, y, $Z_M = 5$ μm) and point forces are calculated at the same (x, y, $z = 0$). Iterations larger than 15 present erratic solutions, but the error on displacements E_r decreases well below the experimental level of noise $\sigma = 0.45$ μm reached at #5 before increasing after #15 (Fig. 5d). This noise level is estimated from direct measurements of bead deformations far from the slug tip at initial times. The behavior is, therefore, intermediate between the two classes of the solutions previously described (Fig. 3a, b). We find again a clear minimum of the proportion of external force $\phi_{ext} = 32\%$ at #5 (Fig. 5d). We previously showed that the force error ΔF is always closed to ϕ_{ext} (Fig. 3). Here, the force error is, therefore, probably close to 30%. Note that this value is fully consistent with the estimates of Fig. 4 for $Z_M = 5$ μm, $\sigma_{XY} = 0.45$ μm.

The optimal stress pattern (Fig. 5c) has the same characteristic properties as the stress field calculated from a time averaged deformation field (Rieu et al. 2004). Perpendicular stress is almost absent outside the slug (Fig. 5c–e). The parallel stress profile (Fig. 5f) presents a large positive peak in the slug tip indicating presence of friction. Here we use two bin sizes $\Delta x = 30$ and 60 μm (circles and bullets) to calculate this profile. Finally, note the presence of large fluctuations along the slug axis (i.e., see the difference between the two curves with different bin sizes $\Delta x = 30$ and 60 μm). These fluctuations seem not to be correlated temporally and spatially (Rieu et al. 2005) but we are currently studying them in more detail.

Simulated polarized fibroblast force pattern

We return now to simulations at a smaller spatial scale and with a force pattern consisting of sharp discrete

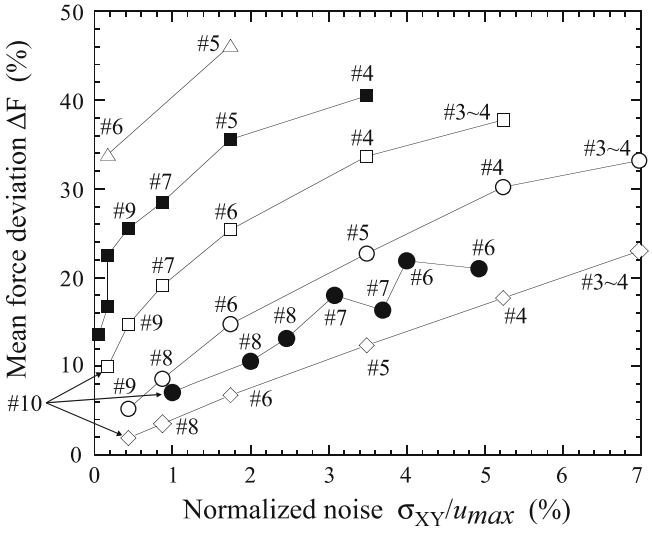

Fig. 4 Force deviation ΔF as a function of the Gaussian noise σ_{XY} normalized by maximal displacement u_{max} and for different values of Δ/Z_M (Δ is the spatial resolution) in case of the slug simulated pattern: $\Delta/Z_M = 1$ (*open triangles*), $\Delta/Z_M = 4/3$ (*closed squares*), $\Delta/Z_M = 2$ (*open squares*), $\Delta/Z_M = 4$ (*circles*), $\Delta/Z_M = 8$ (*diamonds*), and in case of the fibroblast FAs simulated pattern: $\Delta/Z_M = 4$ (*bullets*). We add the iteration number (#) near most of these measurements

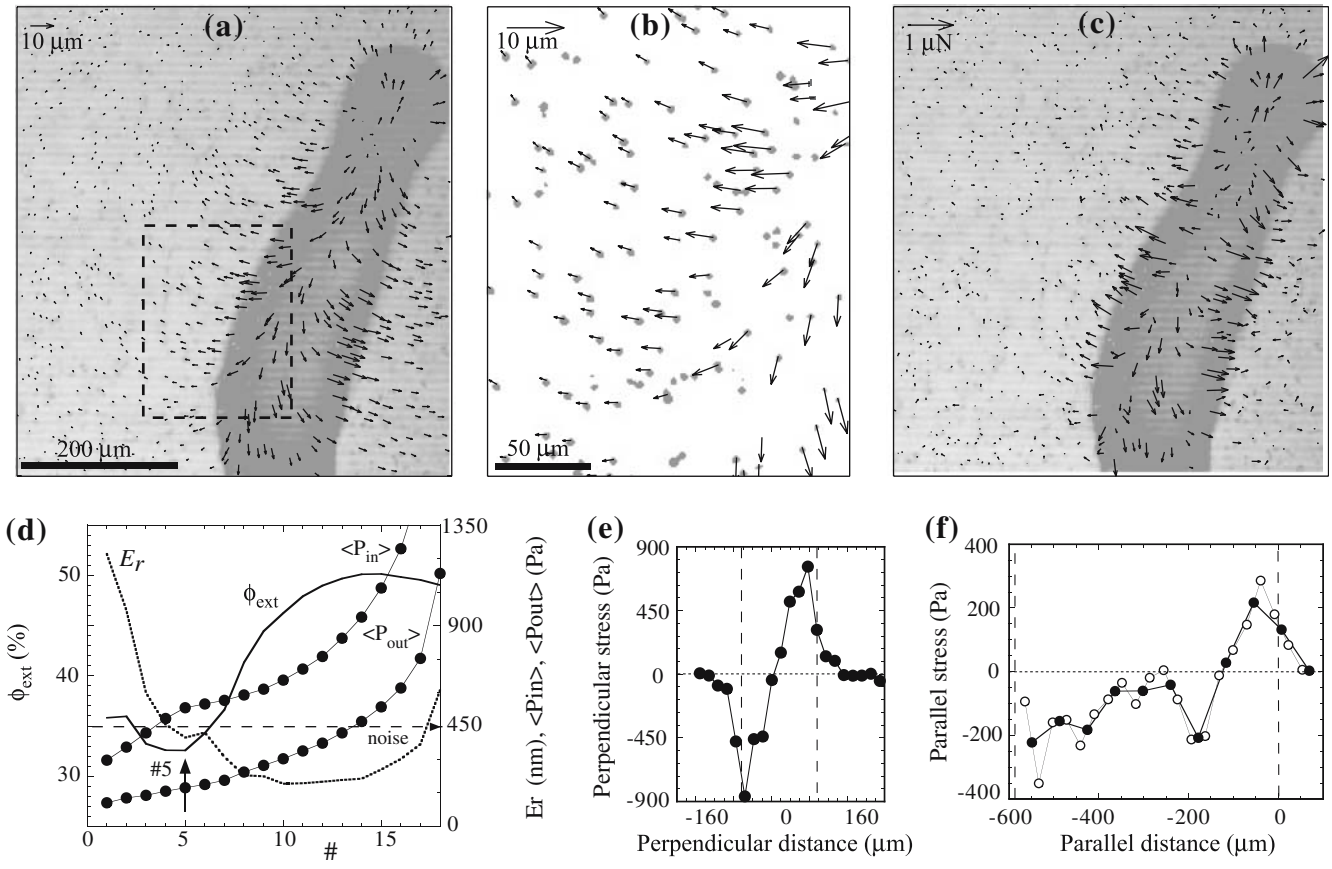

Fig. 5 **a** Deformation field of a *Dictyostelium* slug measured at $Z_M = 5$ µm at a given time superimposed with the slug image. **b** Enlarged part of the deformation field (region inside the *dotted line* of **a**) superimposed with the fluorescence image showing 4 µm beads. **c** Calculated force field at #5. **d** Error landscape as a function of the iteration number #. *Arrow* indicates optimal #. **e**, **f** Perpendicular stress and parallel stress profiles as a function of perpendicular and parallel directions. *Vertical dotted lines* indicate slug boundary. In **f**, *circles* correspond to a bin size $\Delta x = 30$ µm and *bullets* to $\Delta x = 60$ µm for compiling mean stress values from discrete forces at random sites

forces in order to examine the applicability of our method to measure the force exerted by single cells.

This second simulated force pattern mimics traction by a polarized fibroblast with discrete forces exerted only at FA sites separated by $\Delta = 4$ µm (see thick gray arrows in Fig. 6). Forces alternate in magnitude in order to test the resolution of our force reconstruction. Typical force is assumed to be in average 20 nN per FA. This pattern was already simulated recently to demonstrate that in general regularization is needed (Schwarz et al. 2002). This latter study assumed that forces are only localized at the FAs. In our simulations, we do not constrain the force on the FAs, we compute the displacements on a grid with a $\Delta = 4$ µm spacing containing the FAs, and we recalculate the forces after adding noise on the same grid. We use a Young modulus $E = 3.9$ kPa which gives a maximal substrate deformation $u_{max} = 4$ µm at $Z_M = 0.5$ µm and $u_{max} = 2.5$ µm at $Z_M = 1$ µm. In order to find the optimal solution, we use the criterion on the displacement error, $E_r/\sigma_{XY} \sim 1$.

For $Z_M \geq \Delta/2$, it is not possible to find a sharp solution with a reasonable noise. For instance at $Z_M = 2$ µm, the optimal solution spreads the forces at the FAs in three columns even for noise as small as $\sigma_{XY} = 30$ nm which corresponds to a noise to signal ratio σ_{XY}/u_{max} of only 1.2% (Fig. 6a). Here constraining the force inside the cell area (Dembo and Wang 1999; Schwarz et al. 2002) will eliminate such large spreading effect.

For $Z_M = \Delta/4 = 1$ µm, we find a very good agreement with the original force field (including sharpness) for the same level of noise $\sigma_{XY} = 30$ nm (Fig. 6b). When increasing the noise to more realistic values $\sigma_{XY} = 50$ nm and $\sigma_{XY} = 100$ nm (see discussion) at the same Z_M, the solutions are still close to the original force, remain sharp and have the correct amplitude (Fig. 6c, d). The error landscape at $\Delta/Z_M = 4$ appears exactly as the one found for slug type pattern and ΔF is minimum when E_r reaches the level of added noise (Fig. 6e). The relative deviations on forces at the FAs are $\Delta F = 10.6\%$ (#7) and $\Delta F = 21.9\%$ (#6) for $\sigma_{XY} = 50$ nm and $\sigma_{XY} = 100$ nm, respectively. At $\sigma_{XY} = 50$ nm, the mean value of the force noise outside the FAs is 2.2 nN and the histogram of the force noise amplitude is well separated from the histogram of the forces at FAs (Fig. 7a). At a noise level of $\sigma_{XY} = 100$ nm, some scatter in the direction of the force at the FAs appears (Fig. 6d), and the force noise

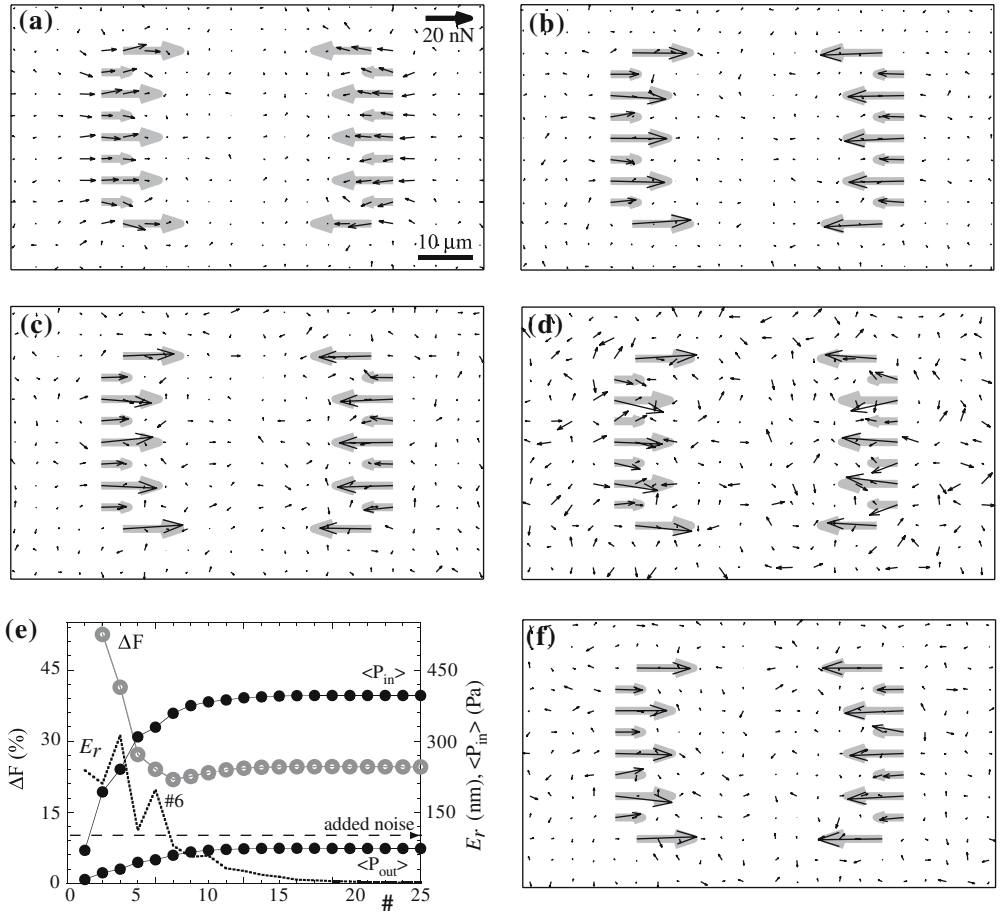

Fig. 6 Reconstructed force patterns of simulated polarized fibroblast are presented. The calculations of the forces are performed for different values of the two important parameters: mean depth Z_M of recorded deformations and Gaussian noise on displacements σ_{XY}. **a** $Z_M = 2$ µm, $\sigma_{XY} = 0.03$ µm; **b** $Z_M = 1$ µm, $\sigma_{XY} = 0.03$ µm; **c** $Z_M = 1$ µm, $\sigma_{XY} = 0.05$ µm; **d** $Z_M = 1$ µm, $\sigma_{XY} = 0.1$ µm; **f** $Z_M = 0.5$ µm, $\sigma_{XY} = 0.15$ µm. Force scale is the same for all patterns. **e** Error landscape for $Z_M = 1$ µm, $\sigma_{XY} = 0.1$ µm

histogram is broader (Fig. 7b). The histograms of the FAs (small force amplitude FA sites) and of noise actually start to overlap. For $Z_M = \Delta/4 = 1$ µm, $\sigma_{XY} = 100$ nm is, therefore, close to the maximal authorized noise. The right side tail of the noise histograms (here about 4.5 nN at $\sigma_{XY} = 50$ nm and 7.5 nN at $\sigma_{XY} = 100$ nm) determines the minimal point like forces that can be reasonably measured.

In Fig. 4, we report the relative force deviation ΔF of the FA simulation as a function of noise to signal ratio for $Z_M = \Delta/4 = 1$ µm ($u_{max} = 2.5$ µm). The curve is qualitatively similar to the slug simulation for the same geometrical ratio Δ/Z_M. This confirms the fact that the results of these simulations can be transposed to other force patterns. Note that the maximal authorized noise is smaller for FAs (5%) than for slugs (7%). Isolated point-like forces of small amplitude are much more sensitive to the surrounding noise than regions of slug with spatially extended forces. For $Z_M = \Delta/8 = 0.5$ µm, we can find as expected a better agreement with the original force for both $\sigma_{XY} = 100$ nm (not shown) and $\sigma_{XY} = 150$ nm (Fig. 6f) with ΔF = 3% and ΔF = 6%, respectively.

Discussion

In recent works (Rieu et al. 2004, 2005)), we calculated for the first time the force exerted by multicellular assemblies (i.e., *Dictyostelium* slugs) migrating on flexible substrates using an iterative biconjugate gradient method. In this article, we address the details of the iterative method and we determine the domain of validity of our method.

This method does not use "explicit" regularization but it might be interpreted as "effectively" introducing some regularization. In classical regularization schemes, constraints are added to impose small or smoothly varying forces in order to kill unrealistic force patterns. Forces are localized to specific positions or regions. Starting from noisy and eventually chaotic solutions, a given regularization parameter is increased until noise is sufficiently filtered out (Dembo and Wang 1999; Schwarz et al. 2002). Our method basically does the same but it proceeds in the other direction: we start from a very smooth estimate (the null solution) and iterate to include more and more information until one stops

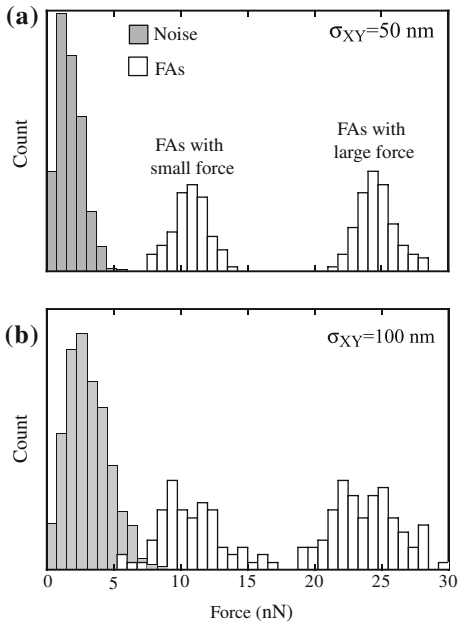

Fig. 7 Histograms of force amplitudes of simulated polarized fibroblast for **a** $Z_M = 5$ μm, $\sigma_{XY} = 0.05$ μm and **b** $Z_M = 5$ μm $\sigma_{XY} = 0.1$ μm. Noise corresponds to the force outside the FA sites

before noise becomes dominant. This is achieved by making use of various possible criteria. The method is particularly simple to implement because it uses localized forces calculated at the same (x, y) coordinates as the measured deformations. Methods using stress fields (i.e., smeared out forces over a given mesh unit cell area) are much more complicated (Dembo et al. 1996).

Our method is an unconstrained method as we do not assign zero forces outside the cell or slug area (Butler et al. 2002). Of course, the internal force might be slightly biased by the substantial remaining outside force. On the other hand, if we constrained the solution, we could miss the important forces remaining in the slime sheath trail of the slug (Rieu et al. 2005). In case of single cells, one may miss forces arising from the thin and fast moving filipodia that are hardly visible under common microscope configurations. The presence of forces outside their supposed location also allows one to examine quickly if data collection suffers some systematic bias. The latter bias may arise due to elastomer inhomogeneity or presence of forces outside the recorded field of view.

We have simulated different patterns of forces in order to study the influence of the experimental parameters such as the noise or the depth of recorded displacements. We show that, with the experimental parameters used to record the deformation field of a migrating slug (Rieu et al. 2004, 2005)), our solutions (force patterns) are stable and robust. The resulting deviation of the force from the original force field might be as small as few percent which is comparable to methods that use explicit regularization (Schwarz et al. 2002). Therefore, we confirm here what had been implicitly demonstrated; namely that explicit regularization is less relevant for low noise level (Schwarz et al. 2002). On the other hand, our method is not efficient in the following cases: (1) if $\Delta/Z_M < 4$ and the distribution of forces is sharp; (2) if noise is larger than 6% of maximum deformations.

The influence on the force calculations of the ratio Δ/Z_M between the grid spacing Δ and the depth of recorded plane of deformation Z_M was never reported to the best of our knowledge. The larger Δ/Z_M is, the easier is the force calculation (even if noise level is increased). For two very different simulated force fields, we found that the condition $\Delta/Z_M \geq 4$ allows one to find sharp variations of the forces. $\Delta/Z_M = 2$ on the other hand, allows one to measure with a good accuracy all slug profiles. Even $\Delta/Z_M = 1$ does not prevent the estimation of the general shape and the measurement of the mean force values (Fig. 3c). Recently, it is has been suggested that the inverse problem becomes computationally more efficient when being solved in Fourier space (Butler et al. 2002). However, these authors took $Z_M = 0$, thus an infinite Δ/Z_M ratio may account (at least partially) for such efficiency.

In a real space, as it is true in our case, if forces are calculated at the sites of deformation measurements, it gives rise to singular Green functions. Dembo and Wang (1999) used a depth distribution in the interval between $Z_M = 0$ and $Z_M = 2.5$ μm arising from the 5 μm depth of field of their objective. Subsequent improvements in their data collection using image correlation analysis allowed these authors to obtain a spatial resolution of $\Delta = 3$–4 μm (Munevar et al. 2001). With these experimental parameters, $\Delta/Z_M \sim 2.8$ and forces may indeed be greatly spread out especially because their noise to signal ratio is generally larger than the one investigated here. Schwarz et al. on the other hand took $Z_M = 0$ but they did not pick up deformations at the sites (FAs) where forces are calculated (Schwarz et al. 2002). The FAs are separated by $\Delta = 4$ μm. The minimum distance between measured displacements and forces is $d = 2$ μm which plays exactly the same role as Z_M in our method. Their $\Delta/d = 2$ and large noise to signal ratio (i.e., 10%) is clearly out of the range of our method (Fig. 4). But they also show that if Δ is increased to 7 μm (i.e., $\Delta/Z_M = 3.5$), explicit regularization can be neglected in agreement with our finding for $\Delta/Z_M \sim 4$.

We show now that the range of required parameters in our method is accessible experimentally. The first important parameter is the Young's modulus E which has to be adjusted in order to optimize the displacements: they have to be smaller than the spatial resolution Δ but large enough to obtain a larger signal to noise ratio. As lateral noise σ_{XY} is almost independent of absolute deformations (see below), decreasing E increases the signal to noise ratio. In case of polyacrylamide substrate, E may be adjusted by trial and error methods in the range 0.2–50 kPa by changing the proportion of acrylamide and *bis* monomers (Pelham and Wang 1997).

The lateral noise σ_{XY} might be optimized in several ways. A large bead diameter ϕ greatly reduces the uncertainty in the bead centroid. Indeed, theoretically, one can expect an error $\delta \sim 1/(2\phi)$ (in pixels) on the bead centroid when the bead size increases by 1 pixel due to blinking. The bead displacement is a difference between two positions. The bead displacement error σ is nearly twice the value of δ. ϕ, however, should stay three- to fivefold smaller than the lateral resolution Δ in order to obtain a homogeneous distribution of mostly isolated beads. For $\Delta = 20$ μm, $\phi = 4$ μm is well suited. By increasing the pixel resolution, it is possible to use smaller beads for the same field of view while keeping the lateral noise constant. Using such 4 μm beads and a pixel resolution of 1 pixel/μm (800×600 pixels typical confocal scans), we measured a lateral noise $\sigma_{XY} =$ 0.45 μm and we could calculate the force solution with an estimated force error $\Delta F = 30\%$ (Fig. 5).

Increasing pixel resolution is possible for instance using the latest generation of five megapixel camera for epifluorescence microscopy or scan sizes up to 4,096×4,096 pixels for recent confocal microscopes. This may allow one to explore smaller Δ with particle tracking algorithms. Alternatively, one may chose to use correlation-based optical flow algorithms practiced for particle image velocimetry (PIV) measurements. This method is now currently implemented to measure the deformation field in flexible substrate experiments at single cell level (Beningo et al. 2001; Munevar et al. 2001; Butler et al. 2002; Marganski et al. 2003). A subpixel accuracy (i.e., 0.1–0.01 pixel) may be obtained using an interpolation algorithm (Westerweel 1997). Therefore, the lateral resolution is generally around 50 nm, a level of noise low enough for our iterative method to find a good solution for $\Delta/Z_M \geq 4$ (Fig. 6b, c).

In principle, the condition $\Delta/Z_M \geq 4$ is not very difficult to fulfill but two limitations may exist depending on the spatial scale of the experiment. In case where one has a very large recorded field of view (e.g., of the order of 1 mm as in case of slugs), it might be difficult to find a homogeneous bead coverage for $Z_M < 5$ μm on the whole image due for instance to substrate roughness. Special care should then be taken in preparing the elastic substrates to minimize this roughness. For single cells experiments, Z_M is generally not limited by the substrate roughness as the field of view is smaller than 100 μm. The depth of field of high numerical aperture oil immersion objective also allows one to investigate the range $Z_M = 0.5 \sim 1$ μm. The lower bound of Z_M derives from the fact that the point-like forces are in fact distributed over a finite size area. Assuming that the distribution of magnitude of force is Hertzian, Schwarz et al. (2002) showed that the point force approximation is justified at a distance which is roughly the size of the force area. In case of single cells, these authors assumed that forces are distributed over the size of the FAs whose lateral extension ranges up to few micrometers (Balaban et al. 2001). However, most of the FAs are roughly 1 μm long and it was also reported that the overall distribution of FAs only partially resembles the distribution of traction stress (Beningo et al. 2001; Reinhart-King et al. 2005). The depth $Z_M = 1$ μm required to obtain a spatial resolution of $\Delta = 4$ μm seems reasonably accessible experimentally.

In conclusion, we have developed a simple iterative method to calculate the force responsible for deformations of flexible substrates. Our method works well as far as the plane of recorded deformation is sufficiently close to the surface and the noise is not too high: requirements that can be fulfilled in experiments. One drawback, compared to explicit regularization techniques, is that those conditions can sometimes be restrictive. However, our computational technique can be implemented with ease to accommodate different situations from single cells to multicellular colonies and also non-biological systems. It can be particularly useful for large fields with more than 1,000 vectors as direct matrix inversion methods as the ones used with regularization methods fail for N larger than a few hundreds.

Acknowledgements J.P.R. acknowledges support from the Japan Society for the Promotion of Science (Invitation Fellowship for Research in Japan, Long Term, FY2002, FY2003, FY2004). The warm hospitality of Pr. S. Iwasaki at Tohoku Institute of Technology is acknowledged. Part of this work was done at Photodynamics Research Center (PRC). We acknowledge Prof. J. Nishizawa and Prof. S. Ushioda for permitting us to use the optical facilities at PRC. We would like also to thank S. Sawai, C. Cottin-Bizonne, L. Bocquet and C. Ybert for helpful comments on the manuscript.

References

Abercrombie M, Dunn GA (1975) Adhesions of fibroblasts to substratum during contact inhibition observed by interference reflection microscopy. Exp Cell Res 92:57–62

Balaban NQ, Schwarz US, Riveline D, Goichberg P, Tzur G, Sabanay I, Mahalu D, Safran S, Bershadsky A, Addadi L, Geiger B (2001) Force and focal adhesion assembly: a close relationship studied using elastic micropatterned substrates. Nat Cell Biol 3:466–472

Beningo KA, Wang YL (2002) Flexible substrata for the detection of cellular traction forces. Trends Cell Biol 12:79–84

Beningo KA, Dembo M, Kaverina I, Small JV, Wang YL (2001) Nascent focal adhesions are responsible for the generation of strong propulsive forces in migrating fibroblasts. J Cell Biol 153:881–888

Butler JP, Tolic-Norrelykke IM, Fabry B, Fredberg JJ (2002) Traction fields, moments, and strain energy that cells exert on their surroundings. Am J Physiol Cell Physiol 282: C595–C605

Dallon JC, Othmer HG (2004) How cellular movement determines the collective force generated by the *Dictyostelium* discoideum slug. J Theor Biol 231:203–222

Dembo M, Wang YL (1999) Stresses at the cell-to-substrate interface during locomotion of fibroblasts. Biophys J 76:2307–2316

Dembo M, Oliver T, Ishihara A, Jacobson K (1996) Imaging the traction stresses exerted by locomoting cells with the elastic substratum method. Biophys J 70:2008–2022

Dormann D, Weijer CJ (2001) Propagating chemoattractant waves coordinate periodic cell movement in *Dictyostelium* slugs. Development 128:4535–4543

Dormann D, Siegert F, Weijer CJ (1996) Analysis of cell movement during the culmination phase of *Dictyostelium* development. Development 122:761–769

Galbraith CG, Yamada KM, Sheetz MP (2002) The relationship between force and focal complex development. J Cell Biol 159:695–705

Haga H, Irahara C, Kobayashi R, Nakagaki T, Kawabata K (2005) Collective movement of epithelial cells on a collagen gel substrate. Biophys J 88:2250–2256

Landau LD, Lifshitz EM (1986) Theory of elasticity, 3rd edn (J. B. Sykes, W. H. Reid, translators). Pergamon Press, Oxford, pp 37–41

Lauffenburger DA, Horwitz AF (1996) Cell migration: a physically integrated molecular process. Cell 84:359–369

Marganski WA, Dembo M, Wang YL (2003) Measurements of cell-generated deformations on flexible substrata using correlation-based optical flow. Methods Enzymol 361:197–211

Mohrdieck C, Wanner A, Roos W, Roth A, Sackmann E, Spatz JP, Arzt E (2005) A theoretical description of elastic pillar substrates in biophysical experiments. Chemphyschem 6:1492–1498

Munevar S, Wang YL, Dembo M (2001) Traction force microscopy of migrating normal and H-ras transformed. Biophys J 80:1744–1757

Pelham RJ, Wang YL (1997) Cell locomotion and focal adhesions are regulated by substrate flexibility. Proc Natl Acad Sci USA 94:13661–13665

Petronis S, Gold J, Kasemo B (2003) Microfabricated force-sensitive elastic substrates for investigation of mechanical cell–substrate interactions. J Micromech Microeng 13:900–913

Press WH, Teukolsky SA, Vetterling WT, Flannery BP (1992) Numerical recipes in FORTRAN 77: the art of scientific computing (vol 1 of Fortran numerical recipies), 2nd edn. Cambridge University Press, Cambridge. http://www.lib-lanl.gov/numerical/index.html

Reinhart-King CA, Dembo M, Hammer DA (2005) The Dynamics and mechanics of endothelial cell spreading. Biophys J. BioFAST, published on April 22, 2005 as DOI 10.1529/biophysj.104.054320

Rieu JP, Upadhyaya A, Glazier JA, Ouchi NB, Sawada Y (2000) Diffusion and deformations of single hydra cells in cellular aggregates. Biophys J 79:1903–1914

Rieu JP, Barentin C, Sawai S, Maeda Y, Sawada Y (2004) Cell movements and mechanical force distribution during the migration of *Dictyostelium* slugs. J Biol Phys 30:345–364

Rieu JP, Barentin C, Maeda Y, Sawada Y (2005) Direct mechanical force measurements during the migration of *Dictyostelium* slugs using flexible substrata. Biophys J 89:3563–3576

du Roure O, Saez A, Buguin A, Austin RH, Chavrier P, Siberzan P, Ladoux B (2005) Force mapping in epithelial cell migration. Proc Natl Acad Sci USA 102:2390–2395

Schwarz US, Balaban NQ, Riveline D, Bershadsky A, Geiger B, Safran SA (2002) Calculation of forces at focal adhesions from elastic substrate data: the effect of localized force and the need for regularization. Biophys J 83:1380–1394

Tan JL, Tien J, Pirone DM, Gray DS, Bhadriraju K, Chen CS (2003) Cells lying on a bed of microneedles: an approach to isolate mechanical force. Proc Natl Acad Sci USA 100:1484–1489

Uchida KS, Yumura S (2004) Dynamics of novel feet of *Dictyostelium* cells during migration. J Cell Sci 117:1443–1455

Uchida KS, Kitanishi-Yumura T, Yumura S (2003) Myosin II contributes to the posterior contraction and the anterior extension during the retraction phase in migrating *Dictyostelium* cells. J Cell Sci 116:51–60

Westerweel J (1997) Fundamentals of digital particle image velocimetry. Meas Sci Technol 8:1379–1392